ChemPubSoc Europe

DOI: 10.1002/chem.201501500

CHEMISTRY A European Journal Full Paper

Single-Molecule Magnets

Analysis of the Role of Peripheral Ligands Coordinated to Zn^{II} in Enhancing the Energy Barrier in Luminescent Linear Trinuclear Zn-Dy-Zn Single-Molecule Magnets

Jean Pierre Costes,*[a] Silvia Titos-Padilla,[b] Itziar Oyarzabal,[c] Tulika Gupta,[d] Carine Duhayon,[a] Gopalan Rajaraman,*[d] and Enrique Colacio*[b]

Abstract: Three new Dy complexes have been prepared according to a complex-as-ligand strategy. Structural determinations indicate that the central Dy ion is surrounded by two LZn units (L^{2-} is the di-deprotonated form of the N_2O_2 compartmental *N,N′*-2,2-dimethylpropylenedi(3-methoxysalicylideneiminato) Schiff base. The Dy ions are nonacoordinate to eight oxygen atoms from the two L ligands and to a water molecule. The Zn ions are pentacoordinate in all cases, linked to the N_2O_2 atoms from L, and the apical position of the Zn coordination sphere is occupied by a water molecule or bromide or chloride ions. These resulting complexes, formulated (LZnX)-Dy-(LZnX), are tricationic with X = H_2O and monocationic with X = Br or Cl. They behave as field-free single-molecule magnets (SMMs) with effective energy barriers (U_{eff}) for the reversal of the magnetization of 96.9(6) K with $\tau_0 = 2.4\times10^{-7}$ s, 146.8(5) K with $\tau_0 = 9.2\times10^{-8}$ s, and 146.1(10) K with $\tau_0 = 9.9\times10^{-8}$ s for compounds with Zn–OH_2, Zn–Br, and Zn–Cl motifs, respectively. The Cole–Cole plots exhibit semicircular shapes with α parameters in the range of 0.19 to 0.29, which suggests multiple relaxation processes. Under a dc applied magnetic field of 1000 Oe, the quantum tunneling of magnetization (QTM) is partly or fully suppressed and the energy barriers increase to $U_{eff} = 128.6(5)$ K and $\tau_0 = 1.8\times10^{-8}$ s for **1**, $U_{eff} = 214.7$ K and $\tau_0 = 9.8\times10^{-9}$ s for **2**, and $U_{eff} = 202.4$ K and $\tau_0 = 1.5\times10^{-8}$ s for **3**. The two pairs of largely negatively charged phenoxido oxygen atoms with short Dy–O bonds are positioned at opposite sides of the Dy^{3+} ion, which thus creates a strong crystal field that stabilizes the axial $M_J = \pm 15/2$ doublet as the ground Kramers doublet. Although the compound with the Zn–OH_2 motifs possesses the larger negative charges on the phenolate oxygen atoms, as confirmed by using DFT calculations, it exhibits the larger distortions of the DyO_9 coordination polyhedron from ideal geometries and a smaller U_{eff} value. Ab initio calculations support the easy-axis anisotropy of the ground Kramers doublet and predict zero-field SMM behavior through Orbach and TA-QTM relaxations via the first excited Kramers doublet, which leads to large energy barriers. In accordance with the experimental results, ab initio calculations have also shown that, compared with water, the peripheral halide ligands coordinated to the Zn^{2+} ions increase the barrier height when the distortions of the DyO_9 have a negative effect. All the complexes exhibit metal-centered luminescence after excitation into the UV π–π^* absorption band of ligand L^{2-} at $\lambda = 335$ nm, which results in the appearance of the characteristic Dy^{III} ($^4F_{9/2}\rightarrow{}^6H_{J/2}$; $J = 15/2$, 13/2) emission bands in the visible region.

Introduction

Lanthanide coordination compounds have been studied extensively in recent years because of their exciting magnetic[1] and photophysical properties.[2] Specifically, they have fuelled research activity in the field of molecular magnetism due to their ability to behave as single-molecule magnets (SMMs)[1a–k] and low-temperature molecular magnetic coolers (MCCs).[1a–p]

[a] *Dr. J. P. Costes, Dr. C. Duhayon*
Laboratoire de Chimie de Coordination
205, route de Narbonne, 31077 Toulouse (France)
E-mail: jean-pierre.costes@lcc-toulouse.fr

[b] *Dr. S. Titos-Padilla, Prof. E. Colacio*
Departamento de Química Inorgánica
Facultad de Ciencias, Universidad de Granada
Av. Fuentenueva S/N, 18071 Granada (Spain)
E-mail: ecolacio@ugr.es

[c] *I. Oyarzabal*
Departamento de Química Aplicada
Facultad de Química, Universidad del País Vasco
UPV/EHU, Paseo Manuel Lardizabal, n° 3
20018 Donostia-San Sebastián (Spain)

[d] *T. Gupta, Prof. G. Rajaraman*
Department of Chemistry
Indian Institute of Technology Bombay Powai
Mumbai 400076 (India)
E-mail: rarajaman@chem.iitb.ac.in

Supporting information for this article is available on the WWW under http://dx.doi.org/10.1002/chem.201501500.

SMMs are molecular coordination compounds that exhibit slow relaxation of magnetization and magnetic hysteresis below a blocking temperature (T_B) and, therefore, they behave as superparamagnetic single-domain nanoparticles. These nanomagnets have outstanding potential applications in fields such as molecular spintronics,[3] ultrahigh density magnetic information storage,[3,4] and quantum computing at the molecular level.[5] The SMM behavior is tied to the existence of an energy barrier (U) that prevents reversal of the molecular magnetization when the polarizing field is removed and leads to magnetic bistability at low temperatures (parallel/antiparallel orientation of the magnetization along the applied field). To enlarge the energy barrier and, therefore, improve the SMM properties, systems with large magnetic anisotropy are required. Lanthanide complexes meet these requirements because they exhibit strong magnetic anisotropy, which arises from a combination of large magnetic moments, strong spin-orbit coupling, and crystal-field effects.[1b] The suitability of lanthanide ions (and actinides) for constructing SMMs has been demonstrated by the large number 3d/4f clusters[6] and low-nuclearity 4f metal complexes[1a–k] that exhibit slow relaxation of the magnetization, most of which contain Dy^{3+} ions. Because heteronuclear 3d/4f clusters generally show modest U values, mainly due to the weakness of the 3d–Ln magnetic exchange couplings, research efforts in this area have been focused on homonuclear Ln and Zn/Ln complexes, which have been reported to exhibit slow relaxation of the magnetization with U and T_B values as high as 652 cm^{-1} and 14 K, respectively.[7,8] With regard to the Zn/Ln complexes, recent experimental results and theoretical calculations have shown that reported ZnDy complexes have, in general, higher U_{eff} values than their MDy (M = Co and Ni) and homonuclear Dy counterparts.[9] This could be due to two factors: 1) the attenuation of the intermolecular magnetic interactions provoked by the presence of diamagnetic Zn^{II} ions (some kind of magnetic dilution) and 2) an increase in electron density on the oxygen donor atoms that connect the Zn^{II} and Dy^{III} ions, provoked by coordination to Zn^{II}. This second factor in turn induces a large electrostatic interaction on the lanthanide ion, which gives rise to a destabilization of the excited states and, as a result, an increase in U_{eff}. This hypothesis was recently supported by some of us by using theoretical calculations.[9g] In connection with this, it should be remarked that the electron density of donor atoms coordinated to the Dy^{III} plays a crucial role in determining the SMM behavior of Dy-containing complexes. This is because axial crystal fields, in which the donor atoms with the largest electron densities are located above and below the equatorial plane, favor the adoption of a $M_J = \pm 15/2$ Kramers doublet ground state (the repulsive interactions between the ligands and the oblate f electrons charge cloud are minimized), leading to easy-axis anisotropy and the SMM behavior.[1b] Therefore, the replacement of a ligand in the Zn^{II} coordination sphere by another ligand with different donor capabilities could affect the electron density on the oxygen bridging atoms and thus the U_{eff} value.

Herein, we describe the syntheses, crystal structures, and detailed ac and dc magnetic properties of three cationic Zn-Dy-Zn complexes, $[(LZn(H_2O))_2Dy(H_2O)](CF_3SO_3)_3$ (**1**), $[(LZnBr)_2Dy(H_2O)](ClO_4)$ (**2**), and $[(LZnCl)_2Dy(H_2O)](ClO_4)(MeOH)$ (**3**; H_2L is the N_2O_2 compartmental ligand *N*,*N*′-2,2-dimethylpropylenedi(3-methoxysalicylideneiminato), see Scheme 1), which mainly differ in the co-ligands coordinated to the Zn^{2+} ions (Cl^-, Br^-, H_2O) and counterions (perchlorate or triflate). Moreover, the new Zn-Dy-Zn complexes, in a similar manner to other Schiff-base Zn/Dy complexes[10] in which the L^{2-} ligand is able to act as an antenna group and sensitize the Ln^{III}-based luminescence, should exhibit interesting luminescent properties. Therefore, these Zn-Dy-Zn complexes could behave as bifunctional materials and combine SMM and luminescent properties.

Experimental Section

Materials

The starting Schiff-base zinc complex $LZn{\cdot}2H_2O$,[11] (L^{2-} = *N*,*N*′-2,2-dimethylpropylenedi(3-methoxysalicylideneiminato)) was prepared as previously described. $DyCl_3{\cdot}5H_2O$ and $Dy(CF_3SO_3)_3$ (Aldrich) were used as purchased. High-grade solvents, acetone (Normapur, VWR), methanol (Normapur, VWR), and dichloromethane (Lab reagent grade, Fisher) were used.

Caution! Perchlorate salts of organic or coordination cations are potentially explosive and should be prepared only in small amounts and handled with care.

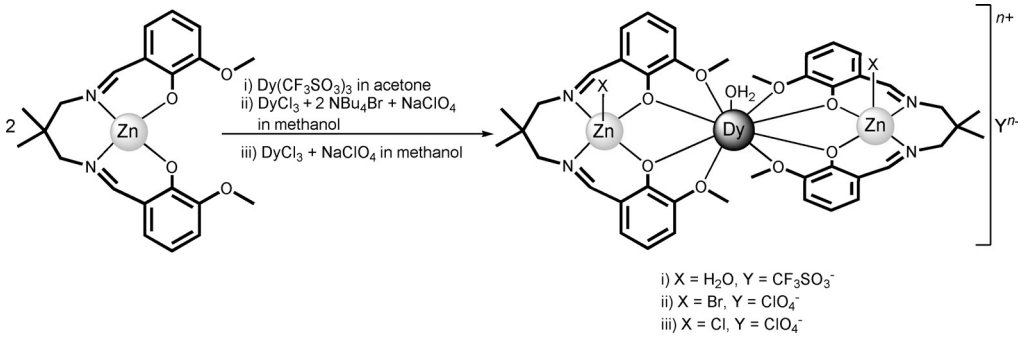

Scheme 1. Synthesis of complexes **1**–**3**.

$[(LZn(H_2O))_2Dy(H_2O)](CF_3SO_3)_3$ (1)

A mixture of $LZn{\cdot}2H_2O$ (0.24 g, 5×10^{-4} mol) and $Dy(CF_3SO_3)_3$ (0.15 g, 2.5×10^{-4} mol) in acetone (15 mL) was stirred for 30 min and then filtered. The solution was concentrated to 5 mL. Slow diffusion of dichloromethane into the acetone solution gave crystals suitable for X-ray analysis, which were filtered off and dried (yield: 0.30 g, 78%). IR (ATR): $\tilde{\nu}=3304$ m, 2956 w, 1708 w, 1642 m, 1627 s, 1609 w, 1563 w, 1473 s, 1437 m, 1395 w, 1282 s, 1240 s, 1219 s, 1166 s, 1078 w, 1064 m, 1027 s, 967 w, 928 w, 848 w, 736 m, 636 cm^{-1} m; elemental analysis calcd (%) for $C_{45}H_{54}DyF_9N_4O_{20}S_3Zn_2$ (1531.40): C 35.29, H 3.55, N 3.66; found: C 35.02, H 3.39, N 3.61.

$[(LZnBr)_2Dy(H_2O)](ClO_4)$ (2)

A mixture of $LZn{\cdot}2H_2O$ (0.47 g, 1×10^{-3} mol), $DyCl_3{\cdot}5H_2O$ (0.18 g, 5×10^{-4} mol), Bu_4NBr (0.32 g, 1×10^{-3} mol) and $NaClO_4$ (0.07 g, 5×10^{-4} mol) in methanol (30 mL) was stirred and heated for 30 min and then filtered off. The solution was left to stand and the crystals that appeared after 5 d were filtered off and dried (yield: 0.5 g, 76%). IR (ATR): $\tilde{\nu}=3524$ w, 3371 m, 2965 w, 2944 w, 1639 m, 1627 s, 1608 w, 1566 w, 1469 s, 1435 m, 1416 m, 1393 w, 1292 m, 1282 m, 1244 m, 1223 s, 1170 w, 1078 m, 1062 s, 1019 m, 967 m, 928 w, 847 w, 735 m, 641 cm^{-1} w; elemental analysis calcd (%) for $C_{42}H_{50}Br_2ClDyN_4O_{13}Zn_2$ (1307.40): C 38.58, H 3.85, N 4.29; found: C 38.35, H 3.81, N 4.23.

$[(LZnCl)_2Dy(H_2O)](ClO_4){\cdot}1.25\,MeOH$ (3)

The experimental process used for complex **2** was repeated without addition of Bu_4NBr. The resulting filtered solution was left to stand and the crystals that appeared after 5 d were filtered off and dried (yield: 0.45 g, 70%). IR (ATR): $\tilde{\nu}=3534$ w, 3365 m, 2966 w, 2944 w, 1639 m, 1626 s, 1608 w, 1566 w, 1469 s, 1435 m, 1416 m, 1392 w, 1293 m, 1282 m, 1244 m, 1223 s, 1170 w, 1078 m, 1063 s, 1020 m, 967 m, 929 w, 847 w, 736 m, 641 cm^{-1} w; elemental analysis calcd (%) for $C_{43.25}H_{54}Cl_3DyN_4O_{14.25}Zn_2$ (1250.56): C 41.27, H 4.4, N 4.45; found: C 40.95, H 4.32, N 4.28.

Physical measurements

Elemental analyses were carried out at the Laboratoire de Chimie de Coordination Microanalytical Laboratory in Toulouse, France, for C, H, and N. IR spectra were recorded by using a Perkin–Elmer Spectrum 100FTIR in the ATR mode. Magnetic data were obtained by using a Quantum Design MPMS SQUID XL-5 susceptometer and Physical Properties Measurement System PPMS 6000. All samples were pellets (3 mm diameter) molded from ground crystalline samples. Magnetic susceptibility measurements were performed in a 2–300 K temperature range in a 0.1 T applied magnetic field, and diamagnetic corrections were applied by using Pascal's constants.[12] Isothermal magnetization measurements were performed up to 5 T at 2 K. ac susceptibility measurements under different applied static fields were performed by using an oscillating ac field of 3.5 Oe and ac frequencies that ranged from 10 to 10000 Hz.

Crystallographic data collection and structure determination for 1, 2, and 3

Crystals of **1**, **2**, and **3** were kept in the mother liquor until they were dipped into oil. The chosen crystals were mounted on a Mitegen micromount and quickly cooled to 180 (**1**) or 100 K (**2**, **3**). The selected crystals of **1** (colorless, $0.20\times0.20\times0.15$ mm^3), **2** (yellow, $0.30\times0.20\times0.20$ mm^3), and **3** (pale yellow, $0.25\times0.25\times0.10$ mm^3) were mounted on an Oxford-Diffraction Gemini (**1**, **2**) or a Bruker Kappa Apex II (**3**) with a graphite monochromator ($\lambda=0.71073$ Å) and equipped with an Oxford Cryosystems cooler device. The unit cell determination and data integration were carried out by using CrysAlis RED or SAINT packages.[13–15] The structures were solved by using SUPERFLIP[16] and refined by using least-squares procedures in the software package CRYSTALS.[17] Atomic scattering factors were taken from the international tables for X-ray crystallography.[18] Hydrogen atoms were refined by using a riding model. All nonhydrogen atoms were anisotropically refined, excluding counterions and solvent in compound **3**. Treatment with the SQUEEZE facility from PLATON[19] for **1** and **2** resulted in a smooth refinement. Because a few low-order reflections are missing from the data set, the electron count is underestimated. Thus, for complexes **1** and **2**, the values given for ρ_{calcd}, $F(000)$, and the molecular weight are only valid for the ordered part of the structure. Drawings of molecules are performed with the program CAMERON[20] with 30% probability displacement ellipsoids for nonhydrogen atoms.

Crystal data for 1

$C_{45}H_{48}DyF_9N_4O_{20}S_3Zn_2$; $M_r=1525.34$; triclinic; $P\bar{1}$ (No. 2); $Z=4$; $a=16.2920(2)$, $b=17.0861(2)$, $c=24.3926(3)$ Å; $\alpha=103.4874(12)$, $\beta=90.1308(11)$, $\gamma=91.2840(11)^\circ$; $V=6600.95(16)$ $Å^3$; 147103 collected reflections, 32701 unique reflections ($R_{int}=0.048$); 1507 parameters, $R=0.060$, $R_w=0.057$ for 24504 contributing reflections [$I>3\sigma(I)$].

Crystal data for 2

$C_{42}H_{50}Br_2ClDyN_4O_{13}Zn_2$; $M_r=1307.40$; monoclinic; $C2$; $Z=8$; $a=37.6050(9)$, $b=16.6758(2)$, $c=18.3719(4)$ Å; $\beta=114.937(3)^\circ$; $V=10446.8(4)$ $Å^3$; 134774 collected reflections, 29359 unique reflections ($R_{int}=0.046$), 1160 parameters, $R=0.064$, $R_w=0.072$ for 25372 contributing reflections [$I>3\sigma(I)$].

Crystal data for 3

$C_{43.25}H_{55}Cl_3DyN_4O_{14.25}Zn_2$; $M_r=1258.55$; monoclinic; $C2$; $Z=8$; $a=37.5577(13)$, $b=16.6216(5)$, $c=18.2100(6)$ Å; $\beta=114.838(2)^\circ$; $V=10316.4(6)$ $Å^3$; 123848 collected reflections, 36971 unique reflections ($R_{int}=0.024$), 1152 parameters, $R=0.035$, $R_w=0.037$ for 31902 contributing reflections [$I>3\sigma(I)$].

CCDC 1059377 (**1**), 1059378 (**2**), and 1059379 (**3**) contain the supplementary crystallographic data for this paper. These data are provided free of charge by The Cambridge Crystallographic Data Centre.

Computational methodology

The MOLCAS 7.8 program package was used to perform post-Hartree–Fock ab initio calculations.[21] By using multiconfigurational approach, relativistic effects were treated in two steps based on the Douglas–Kroll Hamiltonian. For the generation of basis sets, scalar terms were included that have been used to determine spin-free wavefunctions and also energies through the use of the complete active space self-consistent field (CASSCF) method.[22] Thus, spin-orbit free states were obtained by employing the RASSCF method whereas spin-orbit coupling has been taken into account by using the RASSI-SO method,[23] which uses CASSCF wavefunctions as the basis sets and multiconfigurational wavefunctions as input states. The resulting wavefunctions and the energies of the molecular multiplets were used for the calculation of the magnetic properties and g tensors of the lowest state by using a specially

designed routine SINGLE-ANISO.[24] As a consequence, the magnetic properties of a single magnetic ion are calculated by a fully ab initio approach in which the spin-orbit coupling is considered non-perturbatively. We have employed an [ANO-RCC[25]…7s6p4d2f] basis set for Dy^{III}, an [ANO-RCC…3s2p] basis set for N, an [ANO-RCC…3s2p] basis set for O, an [ANO-RCC…5s4p2d] basis set for Zn, and an [ANO-RCC…2s] basis set for H throughout our calculations. These ANO-RCC-VDZ basis sets used for all the atoms are taken from the ANO-RCC basis library included in the MOLCAS 7.8 program package. Density functional calculations have been performed by using the Gaussian 09[26] code to analyze the Mulliken charge on complexes(**1**–**3**). We employed the UB3LYP functional along with a double-zeta quality basis set that used the Cundari–Stevens (CS)[27] relativistic effective core potential on the Dy atom and the TZV[28] basis set on the other atoms. A tight SCF (1×10^{-8} E_h) has been employed throughout the calculations.

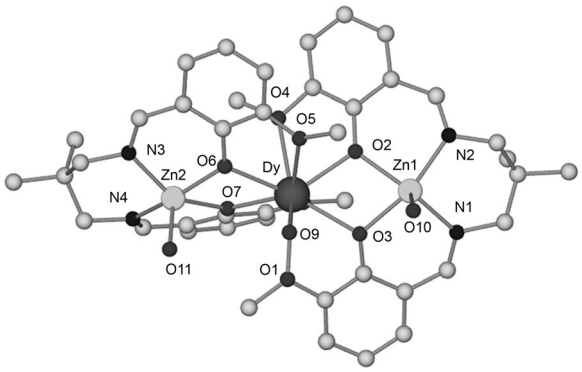

Figure 1. Selected bond lengths [Å] in the Dy1 enantiomer of complex **1**: Dy1–O1: 2.520(3), Dy1–O2: 2.329(3), Dy1–O3: 2.372(3), Dy1–O4: 2.603(3), Dy1–O5: 2.519(3), Dy1–O6: 2.322(3), Dy1–O7: 2.395(3), Dy1–O8: 2.598(3), Dy1–O9: 2.305(3), Zn1–N1: 2.046(4), Zn1–N2: 2.042(5), Zn1–O2: 2.059(3), Zn1–O3: 2.040(3), Zn1–O10: 2.032(4), Zn2–N3: 2.024(4), Zn2–N4: 2.043(4), Zn2–O6: 2.102(3), Zn2–O7: 2.023(3), Zn2–O11: 2.029(3).

Results and Discussion

Complexes **1**–**3** were prepared by using the $ZnL{\cdot}2H_2O$ complex as a ligand for the Dy^{III} ion (see Scheme 1). Thus the reaction between $ZnL{\cdot}2H_2O$ and $Dy(CF_3SO_3)_3$ with a 2:1 Zn^{II}/Dy^{III} molar ratio and acetone as the solvent led to complex **1**. By using $DyCl_3{\cdot}5H_2O$, Bu_4NBr, and $NaClO_4$ as sources of Dy^{III} ions, bromide ligands, and perchlorate counterions, respectively, in a $Zn^{II}/Dy^{III}/Br^-/ClO_4^-$ molar ratio of 2:1:2:1 and methanol as the solvent, complex **2** was obtained. Complex **3** was prepared by following the same method as for **2** but without using Bu_4NBr. All the complexes were obtained in good yield.

The three Zn^{II}-Dy^{III}-Zn^{II} complexes crystallize in triclinic (**1**, $P\bar{1}$, $Z=4$) or monoclinic (**2** and **3**, $C2$, $Z=8$) space groups. The crystallographic data of the three complexes appear in the experimental part and selected bond lengths and angles are collated in the Figure legends. Because complexes **2** and **3** have very similar structures, they present analogous X-ray and magnetic properties. Therefore, hereafter only figures for compound **2** are presented in the main text, whereas figures for **3** are given in the Supporting Information. The structural determination of complex $[(LZn(H_2O))_2Dy(H_2O)](CF_3SO_3)_3$ (**1**) shows the existence of two trinuclear cationic $[(LZnH_2O)_2DyH_2O]^{3+}$ complexes in the asymmetric unit (one being shown in Figure 1 and Figure S1), the charge of which is balanced by three triflate anions that act as counterions.

The $[(LZnH_2O)_2DyH_2O]^{3+}$ is formed by the coordination of two molecules of the LZn complex ligand to the central Dy^{III} ion through the phenoxide oxygen atoms, which bridge Zn^{II} and Dy^{III} ions. In each case, the dysprosium center is nine-coordinate to the four phenoxide bridging groups and the four methoxy oxygen atoms of the two L^{2-} ligands and to a water molecule. The zinc ions are five-coordinate to the N_2O_2 coordination site of the ligand and to a water molecule in the axial position. The three water molecules point in the same direction, with O-Zn-Dy-O torsion angles equal to 17.0(1) and 15.9(1)° in the Dy1 molecule and −19.9(2) and −12.3(2)° in the Dy2 molecule. The six-membered diamino rings appear in a chair conformation after lanthanide complexation, as in the equivalent trinuclear Ni-Ln-Ni complexes.[29] The LZn moieties are not planar, they take an umbrella form with the water molecule pointing above. The related Zn···Dy separations are equal to 3.5445(6) and 3.5756(6) Å in the Dy1 molecule and to 3.5535(6) and 3.5669(6) Å in the Dy2 molecule. The angle between the two O-Dy-O planes that contain the phenoxo oxygen atoms is similar in the two enantiomers (62.6(1)° for Dy1 and 62.5(1)° for Dy2) and the hinge angles, defined as angles between the planes that involve the bridging phenoxide atoms and each metal ion, are slightly different. Thus in the Dy1 molecule the hinge angles between the Zn1-O2-O3, Dy1-O2-O3, and Zn2-O6-O7, Dy1-O6-O7 planes are respectively equal to 23.1(1) and 21.8(1)°, compared with 22.5(1) and 20.3(1)° for the Dy2 molecule. Nevertheless, the Zn···Dy···Zn centers are practically aligned, with Zn···Dy···Zn angles of 175.2(1) and 175.6(1)°. Hydrogen bonds involving the three water molecules linked to the three metal ions and two non-coordinated triflate anions assemble the equivalent trinuclear molecules by pairs, whereas there is no hydrogen bond between different Dy1 and Dy2 molecules. The Dy···Dy separations in the Dy1···Dy1 and Dy2···Dy2 pairs are equal to 9.879(3) and 10.069(4) Å, so the Dy ions are well isolated from each other. Note that the Dy1···Dy2 separation is greater than 12 Å.

The asymmetric unit of complex **2** is again made of two trinuclear Zn-Dy-Zn complexes. The main difference between complexes **1** and **2** is that water molecules linked to the Zn ions have been replaced by bromide ions, so that the trinuclear entities are monocationic, with the formula $[(LZnBr)_2Dy(H_2O)]^+$ (Figure 2 and Figure S2) and a perchlorate anion to ensure electroneutrality. The zinc centers are again pentacoordinate and the Dy ions nonacoordinate. The Br-Zn-Dy-O torsion angles are now equal to −19.4(2) and 127.8(2)° in the Dy1 molecule and 10.2(2), −130.4(2)° in the Dy2 molecule, so a large change is observed in one torsion angle. There is no intermolecular hydrogen bond and only an intramolecular Br···H_2O hydrogen bond that involves the Br ion that points in the same direction as the water molecule linked to the central Dy ion. The net result is that the trinuclear units are well separated from each other, with Dy1···Dy1, Dy2···Dy2, and Dy1···Dy2 separations of 11.434(4), 12.789(4), 11.464(4) Å, respectively.

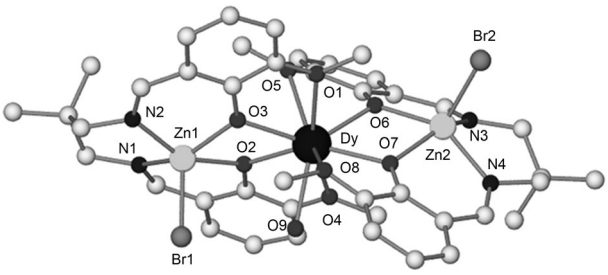

Figure 2. Selected bond lengths [Å] in the Dy1 enantiomer of complex **2**: Dy1–O1: 2.515(5), Dy1–O2: 2.322(5), Dy1–O3: 2.311(5), Dy1–O5: 2.498(5), Dy1–O6: 2.353(5), Dy1–O7: 2.304(5), Dy1–O8: 2.700(5), Dy1–O9: 2.393(6), Dy1–O40: 2.531(6), Dy1–O4: 2.447(6), Zn1–Br1: 2.3352(16), Zn1–N1: 2.066(6), Zn1–N2: 2.058(7), Zn1–O2: 2.065(6), Zn1–O3: 2.113(5), Zn2–Br2: 2.3718(14), Zn2–N3: 2.063(6), Zn2–N4: 2.078(6), Zn2–O6: 2.077(5), Zn2–O: 7.2.111(5).

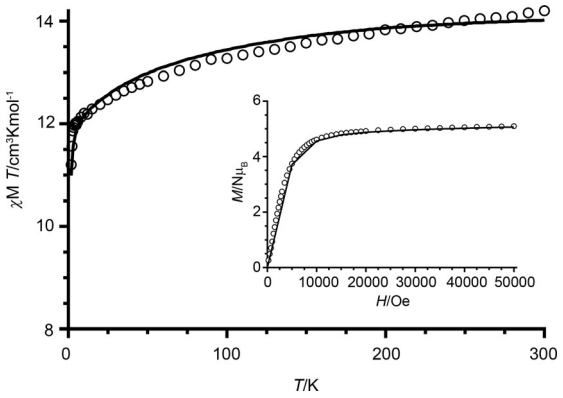

Figure 3. Temperature dependence of $\chi_M T$ and molar magnetization vs. field (inset) for **1**. Solid lines represent the curves calculated by using the ab initio results and taking into account intermolecular interactions.

Complex **3** (Figure S3 in the Supporting Information) is very similar to complex **2**, with chloride ions replacing bromide ions. The Cl-Zn-Dy-O torsion angles are equal to −19.8(1) and 128.8(1)° in the Dy1 molecule and 12.3(1), −130.2(1)° in the Dy2 molecule, identical to those found in complex **2**. There are again intramolecular Cl···H_2O hydrogen bonds in each trinuclear unit, but the presence of an uncoordinated MeOH molecule induces an intermolecular Dy(H_2O)···MeOH···Cl hydrogen bond, which implies the chloride ion not involved in the intramolecular hydrogen bond and connecting the Dy1 and Dy2 molecules. Nevertheless, these Dy1 and Dy2 units are quite well separated by 11.408(3) Å.

Zn polyhedra can be considered as slightly deformed square pyramids, whereas the analysis of the Dy coordination spheres with the "SHAPE" program[30] indicates that in complexes **2** and **3** the spherical tricapped trigonal prism appears to be slightly preferred in comparison to the spherical capped square antiprism, whereas the muffin environment can be retained in complex **1** (see Table S1 in the Supporting Information).

Magnetic properties

The dc magnetic susceptibility measurements of complexes **1**–**3** were performed in the 2 to 300 K temperature range and under an applied magnetic field of 0.1 T (see Figure 3 for **1** and Figure S4 for **2** and **3**). The room-temperature $\chi_M T$ values (14.20, 13.91, and 13.88 $cm^3 K mol^{-1}$ for **1**, **2**, and **3**, respectively) are close to the calculated value of 14.17 $cm^3 K mol^{-1}$ for the ground state of the Dy^{III} ion ($4f^9$, $J=15/2$, $S=5/2$, $L=5$, $g=4/3\ ^6H_{15/2}$) in the free-ion approximation. The thermal variation in $\chi_M T$ for **1**–**3** is very similar; $\chi_M T$ declines smoothly on cooling until approximately 20 K and then sharply reaching a value of approximately 10.80 $cm^3 K mol^{-1}$ at 2 K. The decrease in $\chi_M T$ for **1**–**3** when the temperature is lowered is mainly due to the depopulation of the CF M_J states and possibly very weak intermolecular interactions between the Dy^{III} ions, which could be responsible for the sharp decreases in $\chi_M T$ at very low temperatures. The fact that the $\chi_M T$ value for **2** and **3** starts to decline at higher temperatures than **1** suggests a larger splitting of the $^6H_{15/2}$ ground multiplet.

The field dependence of the magnetization at 2 K for complexes **1**–**3** is very similar and shows a relatively rapid increase at low field without reaching saturation at 5 T, which indicates strong magnetic anisotropy. The magnetization value at the maximum applied field of 5 T (in the 5.1–5.8 $N\mu_B$ range) is lower than that expected for a Dy^{III} ion ($Ms/N\mu_B = g_J J = 10\ N\mu_B$), which is due to the crystal-field effects that lead to a significant magnetic anisotropy. The $\chi'_M T$ value (χ'_M being the in-phase ac susceptibility) at its low-temperature plateau (at 0 and 1000 Oe) is approximately 12.5 $cm^3 mol^{-1} K$ for the three compounds, which agrees well with that expected for randomly oriented crystals with a $M_J = \pm 15/2$ Ising ground Kramers doublet (12.5 $cm^3 mol^{-1} K$).

The dynamic magnetic behavior of compounds **1**–**3** was studied by using ac magnetic susceptibility measurements as a function of the temperature and frequency under 0 and 1000 Oe applied dc magnetic fields. In the absence of an external magnetic field (Figure 4, insets, and Figures S5–S8), all the compounds exhibit frequency dependence of the out-of-phase signal (χ''_M, cf. χ'_M) below 25 K for **1** and below 35.5 K for **2** and **3**, with peaks to 16.5 K and 25 K, respectively, at the maximum frequency of 10000 Hz. This can be attributed to the presence of slow relaxation of the magnetization, indicating that **1**–**3** are SMMs. Both χ'_M and χ''_M components do not go to zero below the maxima at low temperature, which is mainly due to the presence of fast relaxation of the magnetization by a QTM mechanism through the thermal energy barrier between degenerate energy levels. The Cole–Cole plots (Figure S7 in the Supporting Information) in the temperature ranges of 7 to 15 K for **1** and 7 to 27 K for **2** and **3** exhibit semicircular shapes with α parameters in the range of 0.25 to 0.38, 0.21 to 0.27, and 0.19 to 0.29, respectively, which suggests multiple relaxation processes.

The relaxation times (τ) for compounds were extracted from the fitting of the frequency dependence of χ''_M at each temperature to the generalized Debye model (Figure S8 in the Supporting Information). The fit of the high-temperature data to the Arrhenius equation afforded an effective energy barrier

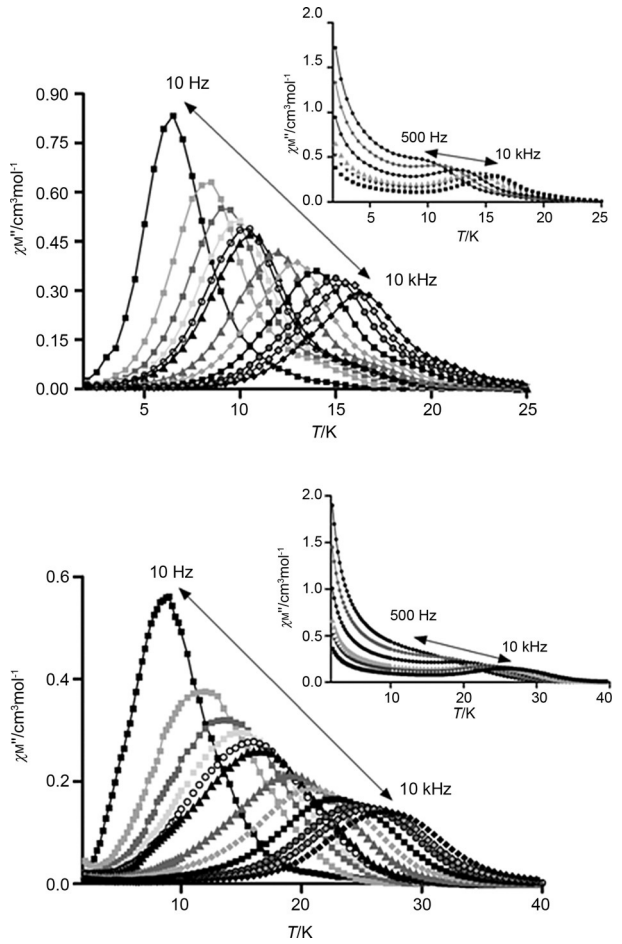

Figure 4. Temperature dependence of out-of-phase χ''_M component of the ac susceptibility for complexes **1** (top) and **2** (bottom) measured under zero (insets) and 1000 Oe applied dc field.

for the reversal of the magnetization of 96.9(6) K with $\tau_0 = 2.4 \times 10^{-7}$ s for **1**, 146.8(5) K with $\tau_0 = 9.2 \times 10^{-8}$ s for **2**, and 146.1(10) K with $\tau_0 = 9.9 \times 10^{-8}$ s for **3**. The Arrhenius plots, constructed from the temperatures and frequencies of the maxima observed for the χ''_M signals in Figure 4 and Figure S6, lead to the same results as expected. Because the data deviate from linearity in the low-temperature region mainly due to the existence of the QTM relaxation process, we have fitted the temperature dependence of the relaxation time to the following equation, which includes contributions from quantum tunneling and Orbach thermal processes:

$$\tau^{-1} = {\tau_{QTM}}^{-1} + \tau_0 \exp(-U_{eff}/k_B T)$$

in which ${\tau_{QTM}}^{-1}$ corresponds to the relaxation frequency of the quantum tunneling relaxation process. The fit of the data afforded an effective energy barrier for the reversal of magnetization $U_{eff} = 188.4$ K with $\tau_0 = 2.1 \times 10^{-8}$ s and $\tau_{QTM} = 2.9 \times 10^{-4}$ s for **2** and $U_{eff} = 173$ K with $\tau_0 = 3.7 \times 10^{-8}$ s and $\tau_{QTM} = 2.6 \times 10^{-4}$ for **3**. In the case of **1**, the relaxation time data could not be fitted to the above simple equation, which may be due to the existence of several relaxation processes, including QTM, Raman, and probably various activated processes, in the studied temperature range. The QTM can be partly or fully suppressed by application of a small external dc field, which often results in an increase in the U_{eff}. Thus, when the ac measurements on complexes **1**–**3** were performed in the presence of a small external dc field of 1000 Oe (Figures S9–S12 in the Supporting Information; this field was chosen because the relaxation process was shown to be the slowest under its application), the tails at low temperature almost disappear and the high temperature peaks remain roughly at the same temperatures as those observed under zero dc applied field, that is, in the 6.5 to 16.2 K (10–10000 Hz), 9 to 27 K (10–10000 Hz), and 8.5 to 27.5 K (10–10000 Hz) ranges, respectively (Figure 4 and Figure S10).

The fit of the high-temperature relaxation times to the Arrhenius law (see Figure 5) leads, as expected, to an increase in the thermal energy barrier and a decrease in τ_0 ($U_{eff} = 128.6(5)$ K and $\tau_0 = 1.8 \times 10^{-8}$ s for **1**, $U_{eff} = 214.7$ K and $\tau_0 = 9.8 \times 10^{-9}$ s for **2**, and $U_{eff} = 202.4$ K and $\tau_0 = 1.5 \times 10^{-8}$ s for **3**).

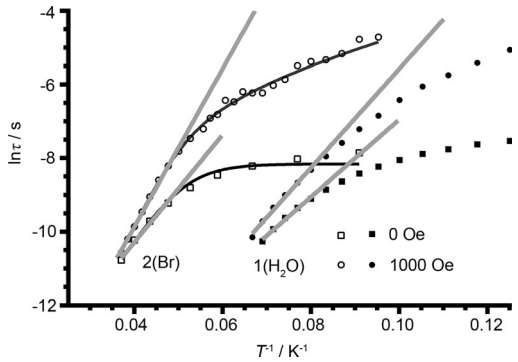

Figure 5. Arrhenius plots (solid grey lines) for the relaxation times (τ) extracted from the χ''_M vs. f data in 0 and 1000 Oe dc fields for compounds **1** (solid symbols) and **2** (open symbols). The black lines correspond to the best fits to QTM plus Orbach (□) and to Raman plus Orbach (○).

Nevertheless, in the case of **2** and **3**, the fact that the experimental relaxation times deviate significantly from the linear Arrhenius model in the 10 to 19 K temperature region under an applied magnetic field of 1 kOe, at which the QTM is almost suppressed, suggests the presence of competing Raman and Orbach processes. The Cole–Cole plots for both compounds (Figure S11 in the Supporting Information) show in the 10 to 27 K temperature regions semicircular shapes with α values in the range of 0.16 to 0.25 for **2** and 0.12 to 0.29 for **3**, which thus confirms the presence of a distribution of relaxation processes in that region. In view of this, we have fitted the experimental data to the following equation, which considers that the spin-lattice relaxation takes place through Raman and Orbach processes:

$$\tau^{-1} = BT^n + {\tau_0}^{-1} \exp(-U_{eff}/k_B T)$$

The first and second terms correspond to the Raman and Orbach processes, respectively. In general, $n = 9$ for Kramers ions,[31] but depending on the structure of the levels, n values

between 1 and 6 can be considered as reasonable.[32] The best fit of the experimental data in the above temperature range affords $n=3.7(1)$, $B=0.02(1)$, $\tau_0=1.5\times10^{-9}$ s, and $U_{eff}=267.4(6)$ K for **2** and $n=2.8(0.6)$, $B=0.2(0.4)$, $\tau_0=3.3\times10^{-8}$, and $U_{eff}=245(4)$ K for **3** (Figure S10, inset, Supporting Information). These results seem to indicate that the Raman relaxation process significantly affects the Orbach relaxation process, which reduces the thermal energy barrier U_{eff} for the magnetization reversal. Data for compound **1** could not be fitted to the above equation, probably due to the existence of Raman and various activated processes, as indicated above.

Ab initio calculations

We have performed ab initio electronic calculations based on the CASSCF + RASSI-SO/SINGLE_ANISO method[22,23] on the X-ray structures by using the MOLCAS 7.8 code[21] with the aim of supporting the presence of axial anisotropy and to gain insight into the mechanism of the slow magnetic relaxation properties of complexes **1**–**3**. In doing so, we also expect to elucidate the role played by the co-ligand coordinated to the Zn^{II} ions (Cl^-, Br^-, H_2O) in determining the magnitude of the energy barrier in these compounds. The Dy^{III} ion has a $^6H_{15/2}$ spin-orbit ground atomic term, which is split by the CF to give eight Kramers doublets (KDs). The calculated g tensors for compounds **1**–**3** are given in Tables S2–S4, whereas their computed orientations are given in Figures S14–S16 in the Supporting Information. The calculated energy spectra of the eight KDs for **1**–**3** span up to 458, 754, and 792 cm^{-1}, respectively (Tables S2–S4 in the Supporting Information). In all three compounds, the subsequent excited states lie at approximately 3100 cm^{-1}. The gap between the ground and adjacent higher excited Kramers doublets (KD1 and KD2) for **2** and **3** (218 and 238 cm^{-1}, respectively) is notably larger than that for compound **1** (92 cm^{-1}). The observed differences in the energy gap could be attributed to the various structural distortions induced by the substitutions in all three complexes, as reflected in the SHAPE analysis. In the three complexes, the ground Kramers doublet (KD1) is calculated to be fundamentally pure $M_J=\pm15/2$ with g tensors values of $g_x=0.02$, $g_y=0.04$, and $g_z=19.57$ for **1**; $g_x=0.00$, $g_y=0.00$, and $g_z=19.94$ for **2**; and $g_x=0.00$, $g_y=0.00$, and $g_z=19.91$ for **3**. The g_z values approach towards the ideally pure $M_J=\pm1/2$ state ($g_z=20$) and, therefore, are almost pure axial (Ising type), which favors the slow relaxation of the magnetization and the SMM behavior.[33] Axiality of the excited states is found to decrease up to the fifth, sixth, and seventh KD for **1**, **2**, and **3**, respectively, with proportional increase in the magnetic moment along the *xy* plane. Beyond these KDs, the energy states increase in axiality to reach almost pure Ising-type characteristics at the highest KD, which reproduces the ground-state observation. This mirror symmetry explicitly represents systems that possess low symmetry around the metal ions. The ground state is found to possess zero magnetic moment (L) in the *xy* plane and it is entirely oriented along the *z* axis. The calculated magnetic moments of the ground state for **1** and **2** (Figure 6, that for **3** is given in Figure S13 in the Supporting Information) lie close to the two shortest Dy–O bonds, as qualitatively predicted by the oblate–prolate model.[1b,9a,b]. In this regard, the electrostatic model[34] has been adopted to calculate the deviation of ab initio computed ground-state g_{zz} orientation with respect to the electrostatic anisotropy axis (see Figures S17–19 in the Supporting Information).

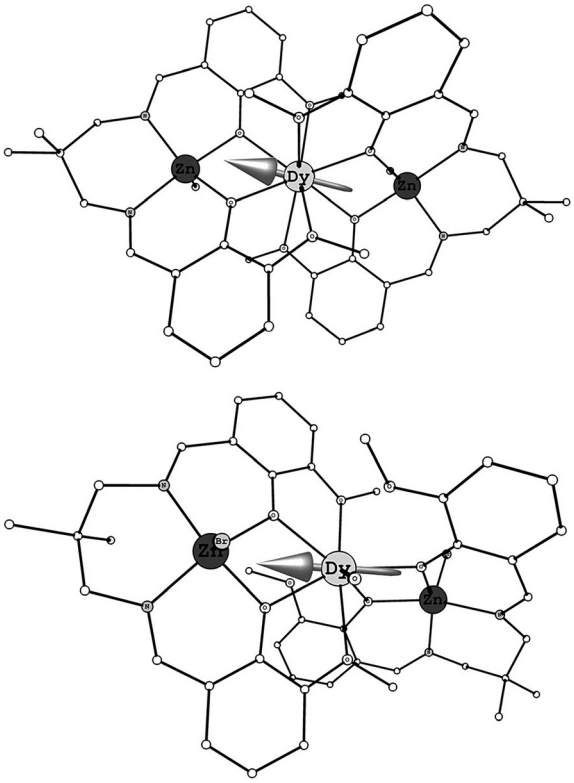

Figure 6. Ab initio computed principal g_{zz} anisotropy orientation for **1** (top) and **2** (bottom).

Because all three compounds possess more than one molecule in the unit cell, we have also performed calculations on the second molecule present in the asymmetric unit (denoted as **1**′, **2**′, and **3**′). The barrier height computed for these molecules are 144, 238, and 218 cm^{-1} for **1**′, **2**′, and **3**′, respectively (see Tables S5–S7 and Figures S20–S23 in the Supporting Information). A large difference is noted for complex **1**, whereas for complexes **2** and **3** the results are very similar. Although the distortion parameters for **1** and **1**′ are same, the large change in the computed U_{calcd} values could be attributed to minor structural alterations around the Dy^{III} ions and also to the orientation of the hydrogen atoms of the water molecule coordinated to the Dy^{III} site, as noted earlier[35] (see Figures S20–S23 in the Supporting Information for orientation of the g_{zz} axis). Because other computed properties (anisotropic axis, electrostatic repulsion, etc.) are same, we have restricted our discussion from here onwards to complexes **1**, **2**, and **3**.

The deviation is found to be extremely small (1.04, 0.73, and 3.19° for **1**, **2**, and **3**, respectively), which implies the tendency of the anisotropy axis to point to the donor atoms with greater electron density and shorter Dy–O bonds (phenoxide bridging groups of the ligands) and forces the oblate electron density

of the Dy^{III} to be perpendicular to them, which thus diminishes electrostatic repulsions (the oblate electron density would lie in the plane of the neutral and more distant methoxy groups and water molecule).[1b] Therefore, the presence of two pairs of large negatively charged phenoxide groups with short Dy–O bonds arranged on opposite sides of the Dy^{III} ion, with the remaining positions occupied by neutral donor oxygen atoms, provide the appropriate crystal field to generate a large energy barrier. The susceptibility and magnetization data calculated by using the anisotropy and CF parameters derived from the ab initio calculations and including weak intermolecular interactions through the mean-field approach with $zJ' = -0.0024$, -0.0025, and $-0.0031\ cm^{-1}$ for **1**, **2**, and **3**, respectively (Figure 3 and Figure S4), agree rather well with the experimental ones, which thus supports the calculated energy spectrum for the eight KDs of these compounds.

To investigate the effect of the Zn^{II} ion, we have performed DFT calculations that reveal larger negative charges on the μ_2-oxo bridged ligand compared with the coordinated neutral oxygen donor atoms (see Tables S8–S10 and Figures S24–S26 in the Supporting Information). Incorporated Zn^{II} ions in all the three complexes induce large polarization on the oxygen atoms, which eventually results in strong electrostatic interactions on the lanthanide ions and reiterates our previous statement.[9g] In our earlier studies on the {ZnDy} complex, the U_{eff} was determined to be 83 cm^{-1}, whereas the barrier heights are much larger in the present set of complexes. This is attributed to the fact that in this set of complexes there are two Zn^{II} ions on both sides of the Dy^{III} ions, which leads to stronger polarization on the phenoxide oxygen atoms and, as indicated above, to large negatively charged phenoxide groups with short Dy–O bonds arranged on opposite sides of the Dy^{III} ion. Stronger polarization and charge distribution on the DyO_8 coordination sphere both induce larger barrier heights. Moreover, the presence of two diamagnetic Zn^{II} ions leads to some internal dilution effects that diminish intermolecular interactions, quench the QTM fast relaxation, and increase the effective energy barrier. All these considerations suggest that incorporation of additional Zn^{II} ions may increase the barrier even further.

It is worth mentioning that the magnetic relaxation in lanthanides is found to occur essentially through the following pathways in the absence of intermolecular interactions:[31,36] 1) through QTM between the ground-state doublet, which occurs due to the large transverse anisotropy of this KD; 2) through the Orbach process, which accounts for relaxation by the excited KDs and occurs essentially due to the non-coincidence of the principal anisotropic axes; 3) through thermally assisted QTM (TA-QTM), which accounts for relaxation through the excited KDs due to their non-Ising nature. The magnitude of these spin-phonon relaxations depend on the square of the transversal magnetic moment. In view of this, and with the aim of disclosing the magnetic pathways in complexes **1**–**3**, we have calculated the mean absolute values of the transverse magnetic moments between connecting pairs of opposite magnetization. As a result of these calculations, the qualitative mechanism of relaxation obtained from ab initio calculations for **1** and **2** are shown in Figure 7 (that of **3** is given in Figure S27 in the Supporting Information), in which the states are arranged according to the values of their magnetic moments. The number at each arrow connecting any two states is the mean absolute value of the matrix elements of the transition magnetic moments between the corresponding states. Due to the almost pure Ising nature of the ground state, QTM is expected to be very weak in all the three complexes. Our computed predictions are supported by the low magnitude of the transversal magnetic moments between the ground-state KDs (10^{-2}, 10^{-3} μ_B for **1** and 10^{-3} μ_B for **2** and **3**) and this exemplifies the experimental observation of zero-field SMM characteristics. The g_{zz} axis of first excited state (KD2) deviates by 36, 12, and 20° with respect to that of the ground state for **1**, **2**, and **3**, respectively. This significant non-coincidence of the anisotropic axis for KD1 and KD2 enhances the Orbach relaxation,[7b] which is more important for compound **1**. For all the compounds, the first excited doublet possesses a very small amount of transverse anisotropy. In view of this, both Orbach and TA-QTM relaxations through the first excited KD are operative, but the former would be favored in **1** and the latter in **2** and **3**. The magnetic moment matrix elements for these processes support this prediction. Thus for **1** the computed number for the Orbach relaxation is very similar but slightly

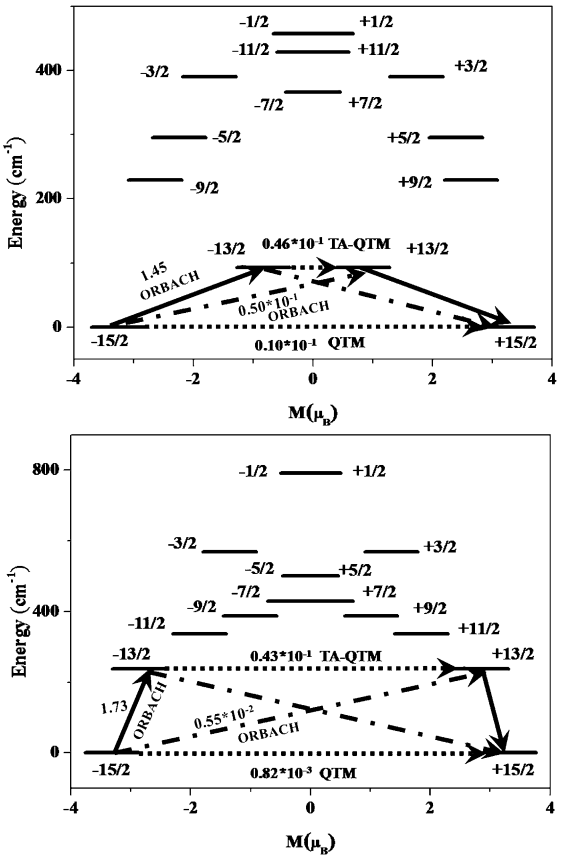

Figure 7. Ab initio computed relaxation mechanism in **1** (top) and **2** (bottom). The thick black lines imply KDs as a function of their magnetic moment along the main anisotropy axis. The dotted lines correspond to ground-state QTM and excited-state TA-QM, solid and dashed dotted lines signify Orbach (Raman) relaxation processes together.

larger than that for TA-QTM relaxation (0.05 μ_B and 0.046 μ_B, respectively), whereas the computed numbers for compounds **2** and **3** are inverted with respect to those of **1** (0.0055 and 0.04 μ_B for Orbach and TA-QTM, respectively, in **2** and 0.0086 and 0.033 μ_B for the same relaxations in **3**).

The calculations find that the ground state Kramers doublet in **1** is predominantly $|\pm15/2>$ (0.98 $|\pm15/2>$), whereas the first excited state is strongly mixed $|\pm13/2>$ (0.37 $|\pm13/2>$ + 0.25 $|\pm11/2>$ + 0.35 $|\pm9/2>$; note that $\pm M_J$ notations in the relaxation mechanism plot are given based on the predominant contribution from $\pm M_J$ energy states). For complexes **2** and **3**, the ground-state KD is predominantly $|\pm15/2>$ (0.99 $|\pm15/2>$). The first excited state is found to be predominantly $|\pm13/2>$ (0.95 $|\pm13/2>$; for complex **3** the coefficient is 0.90). The first excited state of complexes **2** and **3** are found have lesser mixing of other M_J levels compared with that of complex **1**. The mixing of the states is generally correlated to the structural distortion present in the Dy^{III} site. To quantify the distortion, we have performed SHAPE analysis.[30] If tricapped trigonal prism is considered to be the ideal structure, the deviations are noted to be 2.9, 2.1, and 2.0 for complexes **1**, **2**, and **3**, respectively. This clearly reveals that **2** and **3** are more symmetric than complex **1**.

To better understand the relaxation mechanism, we have attempted to use computed crystal-field parameters (Table S11 in the Supporting Information). The corresponding crystal-field Hamiltonian is given as $H_{CF} = B_k^q O_k^q$, in which B_k^q is the crystal-field parameter and O_k^q is the Steven's operator. The QTM contributions are negligible if the non-axial B_k^q ($q \neq 0$ and $k = 2, 4, 6$) terms are smaller than the axial B_k^q ($q = 0$ and $k = 2, 4, 6$) terms, which agrees well with the magnitude of the QTM observed in the relaxation mechanism of all three complexes.

Within complexes **1**–**3**, the axial B_2^0 term is computed to be larger for complexes **2** and **3** than for complex **1**, whereas the non-axial B_2^{-1} term is much larger for complex **1** than for complexes **2** and **3** (see Table S11 in the Supporting Information). This leads to a greater extent of mixing of $\pm M_J$ wavefunctions in complex **1** compared with **2** and **3**. All these cumulative explanations lead to the observation of a larger energy barrier for magnetization reorientation for complexes **2** and **3** as compared with **1**.

The computed energies of the first excited KD for **1** is in close agreement with the experimental results under an applied field of 1000 Oe (when the QTM is almost fully suppressed), whereas those for **2** and **3** are somewhat underestimated. This can be the result of neglected correlation energies and possible small structural changes at low temperatures.[9d, 37] Nevertheless, the reasonably good correspondence between experimental and calculated values supports the proposed mechanism for the relaxation of the magnetization in compounds **1**–**3**. It is notable that we have successfully reproduced the experimental trend of observed energy barriers for magnetization reorientation in these complexes (U_{eff}(**2**) > U_{eff}(**3**) > U_{eff}(**1**)).

With the aim of understanding the effect of the metal-coordinated ligand donation ability, we have performed detailed ab initio calculations by cross comparing the ligands of the three complexes by using a substitution method. To estimate purely the effect of halogen atoms on the calculated barrier height, the structures are not optimized and the Zn–X (X = F, Cl, Br, I) bonds were fixed to known lengths from the literature. Substitution of two coordinated water molecules (coordinated with two Zn^{II} ions) of **1** by F, Cl, Br, I (models **1a**, **1b**, **1c**, and **1d**; see Table 1 and Tables S13–S16 and Figure S28 in the Supporting Information) results pure Ising-type ground-state anisotropy in four models that possess $g_z \approx 20$ expected for the pure $|J = 15/2\ M_J = |\pm15/2>|$ state. This characteristics quenches the QTM completely and, owing to the large deviation of principal magnetization axis (g_z) with respect to the ground state, relaxation is expected to occur through the first excited state and the computed U_{calcd} lies in the range of 101 to 111 cm^{-1} for the four models. Although the difference in U_{calcd} is small, the calculated energy barriers are found to decrease sequentially with a reduction in electronegativity: **1a** (F, 111 cm^{-1}) > **1b** (Cl, 105 cm^{-1}) > **1c** (Br, 104 cm^{-1}) > **1d** (I, 101 cm^{-1}), which corroborates previous observations.[38] Although halogen substitution increases the barrier height, the computed barrier height for models **1b** and **1c** are far away from the U_{calcd} estimate obtained for complexes **2** and **3**. This clearly suggests that structural distortion accompanied by the substitution plays a vital role in enhancing the barrier height rather than the peripheral substitution.

Table 1. Ab initio computed ground-state *g* tensor orientation for all the studied complexes and respective models, along with the associated calculated energy barrier for the reorientation of magnetization.

Complex	Structure	g_{xx}	g_{yy}	g_{zz}	U_{calcd} [cm^{-1}]
$[\{LZn(H_2O)\}_2Dy(H_2O)]^{3+}$	**1**	0.02	0.04	19.57	92.43
$[\{LZn(F)\}_2Dy(H_2O)]^{1+}$	**1a**	0.01	0.01	19.79	111.33
$[\{LZn(Cl)\}_2Dy(H_2O)]^{1+}$	**1b**	0.01	0.01	19.78	105.32
$[\{LZn(Br)\}_2Dy(H_2O)]^{1+}$	**1c**	0.01	0.01	19.78	104.11
$[\{LZn(I)\}_2Dy(H_2O)]^{1+}$	**1d**	0.01	0.01	19.79	101.49
$[\{LZn(Br)\}_2Dy(H_2O)]^{1+}$	**2**	0.00	0.00	19.91	218.06
$[\{LZn(Cl)\}_2Dy(H_2O)]^{1+}$	**3**	0.00	0.00	19.94	238.49

We have performed magnetization hysteresis loop measurements on powdered samples of **1**–**3** at 2 K at a sweeping rate of 0.25 T min^{-1} to confirm the SMM properties of these compounds (Figure 8). All of them exhibit a very similar butterfly-shaped hysteresis loops, but with almost negligible magnetization at zero field (see Figure 8 and Figure S30 for **3**), which is consistent with the QTM generally found for 4f-containing complexes and with the tail that these compounds exhibit at low temperature in the χ''_M versus *T* plot at zero applied field.

As indicated above, the calculated and experimentally extracted effective energy barriers for complexes **1**–**3** follow the order U_{eff} (**1**) < U_{eff} (**2**) ≈ U_{eff} (**3**), which can be mainly due to two factors. First is the deviation of the DyO_9 coordination polyhedron from the ideal geometries. In this regard, it was recently suggested, based on experimental and calculated U_{eff} values for ZnDy complexes, that the structural distortions from ideal geometries decrease the energy barriers.[9g] The results for **1**–**3** agree with this correlation because continued shape

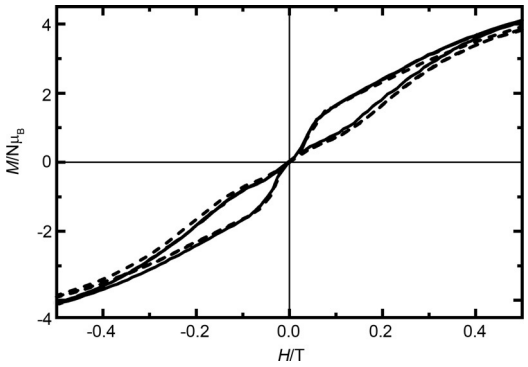

Figure 8. Magnetic hysteresis loops for **1** (solid line) and **2** (dashed line) at 2 K.

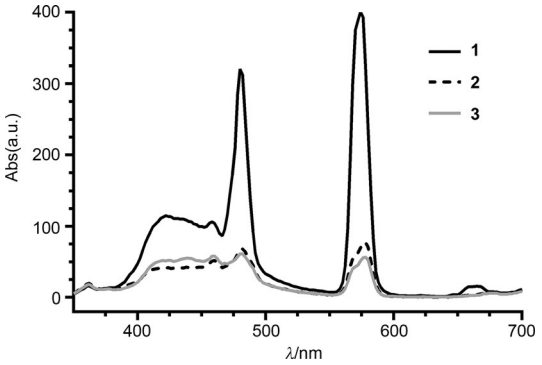

Figure 9. Sensitized emission spectra of complexes **1**–**3** in the solid state at room temperature.

measurements indicate that Dy atoms for **1** present a larger deviation from the ideal geometries TCTPR-9 (spherical tricapped trigonal prism), CASAPRP (spherical capped square antiprism), and MFF-9 (muffin) than complexes **2** and **3** (see Table S1 in the Supporting Information). Second, the electronic effects of the halide co-ligands coordinated to the Zn^{II} ions, which, as supported by DFT calculations on model compounds derived from complex **1** (see Table 1), increase the energy barrier with respect to the coordinated water co-ligand. Nevertheless, the fact that complex **1** exhibits the larger negative charge on phenolate oxygen bridging atoms (see Tables S8–S10 in the Supporting Information) and the smaller U_{eff} value seems to indicate that the first factor has a greater influence in determining the differences in U_{eff} observed for **1**–**3**.

Lanthanide complexes with compartmental Salen-type Schiff-base ligands have been reported to exhibit interesting photophysical properties.[9f,10] These ligands act as antenna groups that sensitize Ln^{III}-based luminescence through an intramolecular energy transfer process. In view of this, the photophysical properties of complexes **1**–**3** have been studied to determine the ability of ligand L^{2-} to act as a sensitizer. In all cases, the photophysical properties of the complexes were studied on microcrystalline powders due to their poor solubility. The reflectance spectrum of the ligand H_2L (Figure S31 in the Supporting Information) shows intense absorption bands in the UV/Vis region located at $\lambda = 214$, 266, 335, and 410 nm. The two former bands are typical of spin-allowed singlet π–π^* electronic transitions in the aromatic groups, the third band is assigned to spin-allowed singlet π–π^* electronic transitions within the C=N groups, and the last is more likely due to an intramolecular ligand charge transfer transition. The absorption spectra of complexes **1**–**3** (Figure S31 in the Supporting Information) show that the latter band disappears upon metal coordination, whereas the other three remain virtually at the same positions as in the ligand. Upon excitation at the ligand energy level ($\lambda_{ex} = 335$ nm), a broad emission appeared (Figure S32 in the Supporting Information) with maxima located at $\lambda_{em} = 530$ nm.

All the complexes exhibit metal-centered luminescence after excitation into the UV π–π^* absorption band of ligand L^{2-} at $\lambda = 335$ nm, which results in the appearance of the characteristic Dy^{III} ($^4F_{9/2} \rightarrow {}^6H_{J/2}$; $J = 15/2$, 13/2) emission bands in the visible region (Figure 9). This sensitized Ln^{III}-based emission can only occur through a L→Ln photoinduced energy transfer process, which probes the ability of ligand L^{2-} to act as an antenna group. However, a significant remaining ligand-centered emission is still observed, which indicates that the energy-transfer process is not complete. It is known that the luminescence observed for the Gd^{3+} complexes is due to the ligand because the lowest excited state for Gd^{3+} is so high in energy that transfer from the ligand is forbidden. The emission spectra for Gd^{3+} complexes that are analogous to **1**–**3** are virtually identical (Figure S32 in the Supporting Information) and show an intense band at $\lambda = 430$ nm, at the same energy as the remnant luminescence of the ligand in the emission spectra of **1**--**3**. The fact that the ligand emits at higher energy upon metal coordination could be attributed to the destabilization of the triplet energy ($^3\pi\pi^*$) level.

Conclusion

Following the complex-as-ligand strategy, we have succeeded in preparing three new Zn^{II}-Dy^{III}-Zn^{II} complexes from the mononuclear complex ZnL ($H_2L = N,N'$-2,2-dimethylpropylenedi(3-methoxysalicylideneiminato) and Dy^{3+}. The new complexes have double phenoxido bridging groups connecting $Zn^{2+}$and Dy^{3+} ions. The Dy^{3+} ion in each compound exhibits a DyO_9 coordination sphere, in which two pairs of largely negatively charged phenoxido groups with short Dy–O bonds are disposed on opposed sides of the Dy^{3+} ion, which thus creates a strong crystal field that could stabilize the axial $M_J = \pm 15/2$ as the ground-state Kramers doublet. Ab initio calculations support the easy-axis anisotropy of the ground-state Kramers doublet and predict zero-field SMM behavior through Orbach and TA-QTM relaxations via the first excited Kramers doublet, which leads to large energy barriers. According to these considerations, the three compounds exhibit zero-field SMM behavior with high thermal energy barriers for the reversal of the magnetization in the 96.9 to 146.8 K range. Under a dc applied magnetic field of 1000 Oe, the QTM is partly or fully suppressed and the energy barriers increase to the 128.6 to 214.7 K range. The large U_{eff} value observed for these Zn^{II}-Dy^{III}-

Zn^{II} complexes is a consequence of the enhancement promoted by the presence of Zn^{2+} ions that induce large charge polarization on the phenoxido oxygen atoms and some dilution effects that diminish intermolecular interactions and quench the QTM fast relaxation. Therefore, the ongoing results suggest that the incorporation of additional Zn^{2+} ions could be a good strategy to additionally increase the barrier. In accordance with the experimental results, ab initio calculations have shown that, compared with water, the peripheral halide ligands coordinated to the Zn^{2+} ions increase the barrier height. The fact that the compound with water as the peripheral ligand coordinated to Zn^{2+} exhibits the larger negative charge on the phenolate oxygen atoms and the smaller U_{eff} value seems to indicate that both the peripheral ligand and the distortion of DyO_9 coordination polyhedron from the ideal geometries (this distortion is larger for the compound with water as the peripheral ligand) play a role in determining the magnitude of U_{eff}.

Acknowledgements

Financial support from the Spanish Ministerio de Ciencia e Innovación (MICINN) (project CTQ-2011-24478 and CTQ2014-56312-P), the Junta de Andalucía (FQM-195, the Project of Excellence P11-FQM-7756), and the University of Granada. I.O. is grateful to the Departamento de Educación, Universidades e Investigación del Gobierno Vasco for a predoctoral fellowship. The authors thank for technical and human support provided by SGIker Medidas Magneticas Gipuzkoa of UPV/EHU. G.R. would like to thank the AISRF and DST Nanomission (SR/NM/NS-1119/2011) for funding. T.G. would like to thank UGC for an SRF fellowship.

Keywords: ab initio calculations · dysprosium · magnetic properties · single-molecule magnets · slow relaxation · trinuclear compounds

[1] a) R. A. Layfield, M. Murugesu (eds), *Lanthanides and Actinides in Molecular Magnetism*, Wiley-VCH, Weinheim, Germany, **2015**; b) J. D. Rinehart, J. R. Long, *Chem. Sci.* **2011**, *2*, 2078 – 2085; c) Y. N. Guo, G. F. Xu, Y. Guo, J. Tang, *Dalton Trans.* **2011**, *40*, 9953 – 9963; d) L. Sorace, C. Benelli, D. Gatteschi, *Chem. Soc. Rev.* **2011**, *40*, 3092 – 3104; e) J. Luzon, R. Sessoli, *Dalton Trans.* **2012**, *41*, 13556 – 13567; f) J. M. Clemente-Juan, E. Coronado, A. Gaita-Ariño, *Chem. Soc. Rev.* **2012**, *41*, 7464 – 7478; g) D. N. Woodruff, R. E. P. Winpenny, R. A. Layfield, *Chem. Rev.* **2013**, *113*, 5110 – 5148; h) P. Zhang, Y.-N. Guo, J. Tang, *Coord. Chem. Rev.* **2013**, *257*, 1728 – 1763; i) F. Habib, M. Murugesu, *Chem. Soc. Rev.* **2013**, *42*, 3278 – 3288; j) R. A. Layfield, *Organometallics* **2014**, *33*, 1084 – 1099; k) B. W. Wang, S. Gao, *The Rare Earth Elements, Fundamental and Applications*, Ed. D. A. Atwood, John Wiley and sons, **2012**, pp. 153 – 160; l) M. Evangelisti, E. K. Brechin, *Dalton Trans.* **2010**, *39*, 4672 – 4676; m) E. Cremades, S. Gomez-Coca, D. Aravena, S. Alvarez, E. Ruiz, *J. Am. Chem. Soc.* **2012**, *134*, 10532 – 10542; n) J. W. Sharples, D. Collison, *Polyhedron* **2013**, *54*, 91 – 103; o) Y.-Z. Zheng, G.-J. Zhou, Z. Zheng, R. E. P. Winpenny, *Chem. Soc. Rev.* **2014**, *43*, 1462 – 1475; p) J.-L. Liu, Y.-C. Chen, F.-S. Guo, M.-L. Tong, *Coord. Chem. Rev.* **2014**, *281*, 26 – 49.

[2] a) M. D. Ward, *Coord. Chem. Rev.* **2007**, *251*, 1663 – 1677; b) K. Binnemans, *Chem. Rev.* **2009**, *109*, 4283 – 4374; c) J.-C. G. Bünzli, *Acc. Chem. Res.* **2006**, *39*, 53 – 61; d) W. C. Chan, D. J. Maxwell, X. Gao, R. E. Bailey, M. Han, S. Nie, *Curr. Opin. Biotechnol.* **2002**, *13*, 40 – 46; e) P. Hänninen, H. Härmä (Eds), *Lanthanide Luminescence, Photophysical, Analytical and Biological Aspects*, Springer-Verlag, Berlin-Heidelberg, **2011**; f) Atwood, D. Ed. The rare Elements: Fundamental and applications, Wiley, **2012**.

[3] L. Bogani, W. Wernsdorfer, *Nat. Mater.* **2008**, *7*, 179 – 186.

[4] a) A. R. Rocha, V. M. García-Suárez, S. W. Bailey, C. J. Lambert, J. Ferrerand, S. Sanvito, *Nat. Mater.* **2005**, *4*, 335 – 339; b) M. Affronte, *J. Mater. Chem.* **2009**, *19*, 1731 – 1737.

[5] a) M. N. Leuenberger, D. Loss, *Nature* **2001**, *410*, 789 – 793; b) A. Ardavan, O. Rival, J. J. L. Morton, S. J. Blundell, A. M. Tyryshkin, G. A. Timco, R. E. P. Winpenny, *Phys. Rev. Lett.* **2007**, *98*, 057201/1 – 057201/4; c) P. C. E. Stamp, A. Gaita-Ariño, *J. Mater. Chem.* **2009**, *19*, 1718 – 1730.

[6] a) R. E. P. Winpenny, *Chem. Soc. Rev.* **1998**, *27*, 447 – 452; b) C. Benelli, D. Gatteschi, *Chem. Rev.* **2002**, *102*, 2369 – 2388; c) R. Sessoli, A. K. Powell, *Coord. Chem. Rev.* **2009**, *253*, 2328 – 2341; d) M. Andruh, J. P. Costes, C. Diaz, S. Gao, *Inorg. Chem.* **2009**, *48*, 3342 – 3359 (Forum Article); e) E. K. Brechin, *Dalton Trans.* **2010**; f) M. Andruh, *Chem. Commun.* **2011**, *47*, 3025 – 3042; g) L. Rosado Piquer, E. C. Sañudo, *Dalton Trans.* **2015**, *44*, 8771 – 8780.

[7] a) C. R. Ganivet, B. Ballesteros, G. de La Torre, J. M. Clemente-Juan, E. Coronado, T. Torres, *Chem. Eur. J.* **2013**, *19*, 1457 – 1465; b) R. J. Blagg, L. Ungur, F. Tuna, J. Speak, P. Comar, D. Collison, W. Wernsdorfer, E. J. L. McInnes, L. F. Chibotaru, R. E. P. Winpenny, *Nat. Chem.* **2013**, *5*, 673 – 678.

[8] a) J. D. Rinehart, M. Fang, W. J. Evans, J. R. Long, *Nat. Chem.* **2011**, *3*, 538 – 542; b) J. D. Rinehart, M. Fang, W. J. Evans, J. R. Long, *J. Am. Chem. Soc.* **2011**, *133*, 14236 – 14239.

[9] a) A. Watanabe, A. Yamashita, M. Nakano, T. Yamamura, T. Kajiwara, *Chem. Eur. J.* **2011**, *17*, 7428 – 7432; b) T. Kajiwara, M. Nakano, K. Takahashi, S. Takaishi, M. Yamashita, *Chem. Eur. J.* **2011**, *17*, 196 – 205; c) M. Maeda, S. Hino, K. Yamashita, Y. Kataoka, M. Nakano, T. Yamamura, T. Kajiwara, *Dalton Trans.* **2012**, *41*, 13640 – 13648; d) J.-L. Liu, Y.-C. Chen, Y.-Z. Zheng, W.-Q. Lin, L. Ungur, W. Wernsdorfer, L. F. Chibotaru, M.-L. Tong, *Chem. Sci.* **2013**, *4*, 3310 – 3316; e) S. Titos-Padilla, J. Ruiz, J. M. Herrera, E. K. Brechin, W. Wersndorfer, F. Lloret, E. Colacio, *Inorg. Chem.* **2013**, *52*, 9620 – 9626; f) M. A. Palacios, S. Titos-Padilla, J. Ruiz, J. M. Herrera, S. J. Pope, E. K. Brechin, E. Colacio, *Inorg. Chem.* **2014**, *53*, 1465 – 1474; g) A. Upadhyay, S. K. Singh, C. Das, R. Mondol, S. K. Langley, K. S. Murray, G. Rajaraman, M. Shanmugam, *Chem. Commun.* **2014**, *50*, 8838 – 8841.

[10] a) W. Y. Bi, X. Q. Lü, W. L. Chai, T. Wei, J. R. Song, S. S. Zhao, W. K. Wong, *Inorg. Chem. Commun.* **2009**, *12*, 267 – 271; b) H. B. Xu, J. Li, L. X. Shi, Z. N. Chen, *Dalton Trans.* **2011**, *40*, 5549 – 5556; c) S. Zhao, X. Liu, W. Feng, X. Lü, W. Y. Wong, W. K. Wong, *Inorg. Chem. Commun.* **2012**, *20*, 41 – 45; d) W. Y. Bi, X. Q. Lü, W. L. Chai, J. R. Song, W. Y. Wong, W. K. Wong, R. A. Jones, *J. Mol. Struct.* **2008**, *891*, 450 – 455; e) S. Zhao, X. Lü, A. Hoy, W. Y. Wong, W. K. Wong, X. Yang, R. A. Jones, *Dalton Trans.* **2009**, *43*, 9595 – 9602; f) W. Feng, Y. Hui, T. Wei, X. Lü, J. Song, Z. Chen, S. Zhao, W. K. Wong, R. A. Jones, *Inorg. Chem. Commun.* **2011**, *14*, 75 – 78; g) G. Muller, C. L. Maupin, J. P. Riehl, H. Birkedal, C. Piguet, J. C. G. Bünzli, *Eur. J. Inorg. Chem.* **2003**, 4065 – 4072; h) T. D. Pasatoiu, C. Tiseanu, A. M. Madalan, B. Jurca, C. Duhayon, *Inorg. Chem.* **2011**, *50*, 5879 – 5889.

[11] a) J. P. Costes, F. Dahan, W. Wernsdorfer, *Inorg. Chem.* **2006**, *45*, 5 – 7; b) B. El Rez, J. P. Costes, C. Duhayon, L. Vendier, J. P. Sutter, *Polyhedron* **2015**, *89*, 213 – 218.

[12] P. Pascal, *Ann. Chim. Phys.* **1910**, *19*, 5 – 70.

[13] *Agilent Technologies (**2011**)*, Agilent Technologies UK Ltd., Oxford, UK. Xcalibur CCD system, CrysAlisPro Software system, Version 1.171.35.19.

[14] *CrysAlis CCD*, *CrysAlis RED and associated programs:* Oxford Diffraction (**2006**). *Program name(s)*. Oxford Diffraction Ltd, Abingdon, England.

[15] *SAINT* Bruker (**2007**). Bruker AXS Inc., Madison, Wisconsin, USA.

[16] *Superflip:* L. Palatinus, G. Chapuis, *J. Appl. Crystallogr.* **2007**, *40*, 786 – 790.

[17] *CRYSTALS*: P. W. Betteridge, J. R. Carruthers, R. I. Cooper, K. Prout, D. J. Watkin, *J. Appl. Crystallogr.* **2003**, *36*, 1487.

[18] International Tables for X-Ray Crystallography, Vol. IV, Kynoch press, Birmingham, England, **1974**.

[19] *SQUEEZE*: P. Van Der Sluis, A. L. Spek, *Acta Crystallogr. Sect. A* **1990**, *46*, 194 – 201.

[20] *CAMERON:* D. J. Watkin, C. K. Prout, L. J. Pearce, (**1996**). Chemical Crystallography Laboratory, Oxford, England.

[21] a) J. A. Duncan, *J. Am. Chem. Soc.* **2009**, *131*, 2416 – 2416; b) F. Aquilante, L. De Vico, N. Ferre, G. Ghigo, P. A. Malmqvist, P. Neogrady, T. B. Pedersen, M. Pitonak, M. Reiher, B. O. Roos, L. Serrano-Andres, M. Urban, V.

Veryazov, R. Lindh, *J. Comput. Chem.* **2010**, *31*, 224 – 247; c) V. Veryazov, P. O. Widmark, L. SerranoAndres, R. Lindh, B. O. Roos, *Int. J. Quantum Chem.* **2004**, *100*, 626 – 635; d) G. Karlström, R. Lindh, P. A. Malmqvist, B. O. Roos, U. Ryde, V. Veryazov, P. O. Widmark, M. Cossi, B. Schimmelpfennig, P. Neograd y, L. Seijo, *Comput. Mater. Sci.* **2003**, *28*, 222 – 239.

[22] P. A. Malmqvist, B. O. Roos, B. Schimmelpfennig, *Chem. Phys. Lett.* **2002**, *357*, 230 – 240.

[23] L. F. Chibotaru, L. J. Ungur, *Chem. Phys.* **2012**, *137*, 064112 – 64112.

[24] a) S. K. Langley, L. Ungur, N. F. Chilton, B. Moubaraki, L. F. Chibotaru, K. S. Murray, *Inorg. Chem.* **2014**, *53*, 4303 – 4315; b) F. Habib, O. R. Luca, V. Vieru, M. Shiddiq, I. Korobkov, S. I. Gorelsky, M. K. Takase, L. F. Chibotaru, S. Hill, R. H. Crabtree, M. Murugesu, *Angew. Chem. Int. Ed.* **2013**, *52*, 11290 – 11293; *Angew. Chem.* **2013**, *125*, 11500 – 11503.

[25] B. O. Roos, R. Lindh, P. A. Malmqvist, V. Veryazov, P. O. Widmark, A. C. Borin, *J. Phys. Chem. A* **2008**, *112*, 11431 – 11435.

[26] M. Frisch, G. W. Trucks, H. B. Schlegel, G. E. Scuseria, M. A. Robb, J. R. Cheeseman, G. Scalmani, V. Barone, B. Mennucci, G. A. Petersson, H. Nakatsuji, M. Caricato, X. Li, H. P. Hratchian, A. F. Izmaylov, J. Bloino, G. Zheng, J. L. Sonnenberg, M. Hada, M. Ehara, K. Toyota, R. Fukuda, J. Hasegawa, M. Ishida, T. Nakajima, Y. Honda, O. Kitao, H. Nakai, T. Vreven, J. A. Montgomery Jr, J. E. Peralta, F. Ogliaro, M. Bearpark, J. J. Heyd, E. Brothers, K. N. Kudin, V. N. Staroverov, R. Kobayashi, J. Normand, K. Raghavachari, A. Rendell, J. C. Burant, S. S. Iyengar, J. Tomasi, M. Cossi, N. Rega, J. M. Millam, M. Klene,J. E. Knox, J. B. Cross, V. Bakken, C. Adamo, J. Jaramillo, R. Gomperts, R. E. Stratmann, O. Yazyev, A. J. Austin, R. Cammi, C. Pomelli, J. W. Ochterski, R. L. Martin, K. Morokuma, V. G. Zakrzewski, G. A. Voth, P. Salvador, J. J. Dannenberg, S. Dapprich, A. D. Daniels, Ö. Farkas, J. B. Foresman, J. V. Ortiz, J. Cioslowski and D. J. Fox, Gaussian 09, Rev. D, 01, Gaussian, Inc.,Wallingford CT, **2009**.

[27] T. R. Cundari, W. J. Stevens, *J. Chem. Phys.* **1993**, *98*, 5555 – 5565.

[28] A. Schäfer, C. Huber, R. Ahlrichs, *J. Chem. Phys.* **1994**, *100*, 5829 – 5835.

[29] J. P. Costes, T. Yamaguchi, M. Kojima, L. Vendier, *Inorg. Chem.* **2009**, *48*, 5555 – 5561.

[30] M. Llunell, D. Casanova, J. Cirera, J. M. Bofill, P. Alemany, S. Alvarez, M. Pinsky, D. Avnir, *SHAPE*, *v1.1b*; University of Barcelona, Barcelona, Spain, **2005**.

[31] A. Abragam, B. Bleaney, *Electron Paramagnetic Resonance of Transition Ions*, Clarendon Press. Oxford, **1970**.

[32] K. N. Shrivastava, *Phys. Status Solidi B* **1983**, *117*, 437 – 458.

[33] H. L. C. Feltham, Y. Lan, F. Klöwer, L. Ungur, L. F. Chibotaru, A. K. Powell, S. Brooker, *Chem. Eur. J.* **2011**, *17*, 4362 – 4365.

[34] N. F. Chilton, D. Collinson, E. J. L. McInnes, R. E. P. Winpenny, A. Soncini, *Nat. Commun.* **2013**, *4*, 2551.

[35] M.-E. Boulon, G. Cucinotta, J. Luzon, C. Degl'Innocenti, M. Perfetti, K. Bernot, G. Calvez, A. Caneschi, R. Sessoli, *Angew. Chem. Int. Ed.* **2013**, *52*, 350 – 354; *Angew. Chem.* **2013**, *125*, 368 – 372.

[36] R. Marx, F. Moro, M. Dörfel, L. Ungur, M. Waters, S. D. Jiang, M. Orlita, J. Taylor, W. Frey, J. van Slageren, *Chem. Sci.* **2014**, *5*, 3287 – 3293.

[37] N. Ishikawa, M. Sugita, T. Ishikawa, S. Koshihara, Y. Kaizu, *J. Phys. Chem. B* **2004**, *108*, 11265 – 11271.

[38] F. Habib, G. Brunet, V. Vieru, I. Korobkov, L. F. Chibotaru, M. Murugesu, *J. Am. Chem. Soc.* **2013**, *135*, 13242 – 13245.

Received: April 17, 2015
Published online on September 11, 2015